Supporting Information

Urotropine-Induced g-C_3N_4 membrane enhancing CO_2 transition for robust and active urea-assisted water splitting

Ze Li[a,1], *Youbin Zheng*[a,1], *Yuze Wang*[a], *Zhenjie Hao*[a], *Yuhui Huang*[a], *Rui Zhu*[b], *Dinghao Zheng*[a], *Ruixia Zhong*[a], *Liang Dong*[a,*], *Jianbing Zang*[b], *Pengfei Li*[a,*], *Zheng-Jun Wang*[c,d,*]

[a] *Key Laboratory of Dielectric and Electrolyte Functional Material Hebei Province, School of Resources and Materials, Northeastern University at Qinhuangdao, Qinhuangdao 066004, China;*
[b] *State Key Laboratory of Metastable Materials Science and Technology, College of Materials Science and Engineering, Yanshan University, Qinhuangdao 066004, China*
[c] *Institute of New Materials and Industrial Technologies, College of Chemistry and Materials Engineering, Wenzhou University, Wenzhou, Zhejiang 325035, China*
[d] *Department of Chemistry, Functional Materials Technische Universität Berlin, 10623 Berlin, Germany*

[*]Corresponding author.
E-mail address: dongliang@neuq.edu.cn (L. Dong), lipengfei@neuq.edu.cn (P. Li), zj0608wang@163.com (Z. Wang).

1. Electrochemical measurements

The electrocatalytic performance was evaluated utilizing a CHI1760E electrochemical workstation equipped with a three-electrode system: a graphite rod serving as the counter electrode, and an Ag/AgCl (3.5 mol/L KCl solution) reference electrode, in a 1 M KOH electrolyte. All recorded potentials were converted to the reversible hydrogen electrode (RHE) using the formula:

$$E_{RHE} = E_{Ag/AgCl} + 0.197 + 0.0591 \times pH$$

Analysis of the current-voltage response was conducted through linear sweep voltammetry (LSV) at a scan rate of 5 $mV \cdot s^{-1}$. Electrochemical impedance behavior was investigated by electrochemical impedance spectroscopy (EIS) over a frequency range from 1 kHz to 0.01 Hz with an AC amplitude of 5 mV. Electrochemical capacitance was determined via cyclic voltammetry (CV) within an 100 mV potential window, employing scan rates of 20, 40, 60, 80, 100, 120, and 140 $mV \cdot s^{-1}$. The stability evaluation of the electrocatalyst was performed using the I-t chronoamperometry method. Tafel slope calculations were carried out utilizing the Tafel equation.

2. Computational detail

In this paper, the modelling of HER process was construct with Ni_3S_2-NiS heterostructure (denoted as NiS_x structure), while the model for OER/UOR were NiOOH surface, as proven by the in-situ Raman spectra. Herein, all calculation was conducted utilizing the CP2K code, a sophisticated tool renowned for its accuracy in quantum mechanical modeling. The simulations were executed employing the Gaussian plane waves (GPW) method, which was complemented by the generalized gradient

approximation (GGA) along with the Perdew-Burke-Ernzerhof (PBE) functional. This combination was instrumental in accurately depicting the potential field that arises from the interaction of valence electrons and atomic nuclei. A cutoff energy of 520 Ry was meticulously chosen to ensure the precision of the calculations. The criteria for the energy convergence were held to a high standard, with a criterion of 1×10^{-6} eV, to guarantee the stability of the calculated energy states. To mitigate the effects of inter-layer van der Waals forces, the unit cell is set to repeat in the XY-direction. For the optimization of the structural models, the Monkhorst-Pack scheme was employed to sample the Brillouin zone. This method, known for its efficiency and accuracy, was used to fine-tune the lattice points, thus ensuring that the resulting structures were optimized to a high degree of accuracy.

Supplementary Figures,

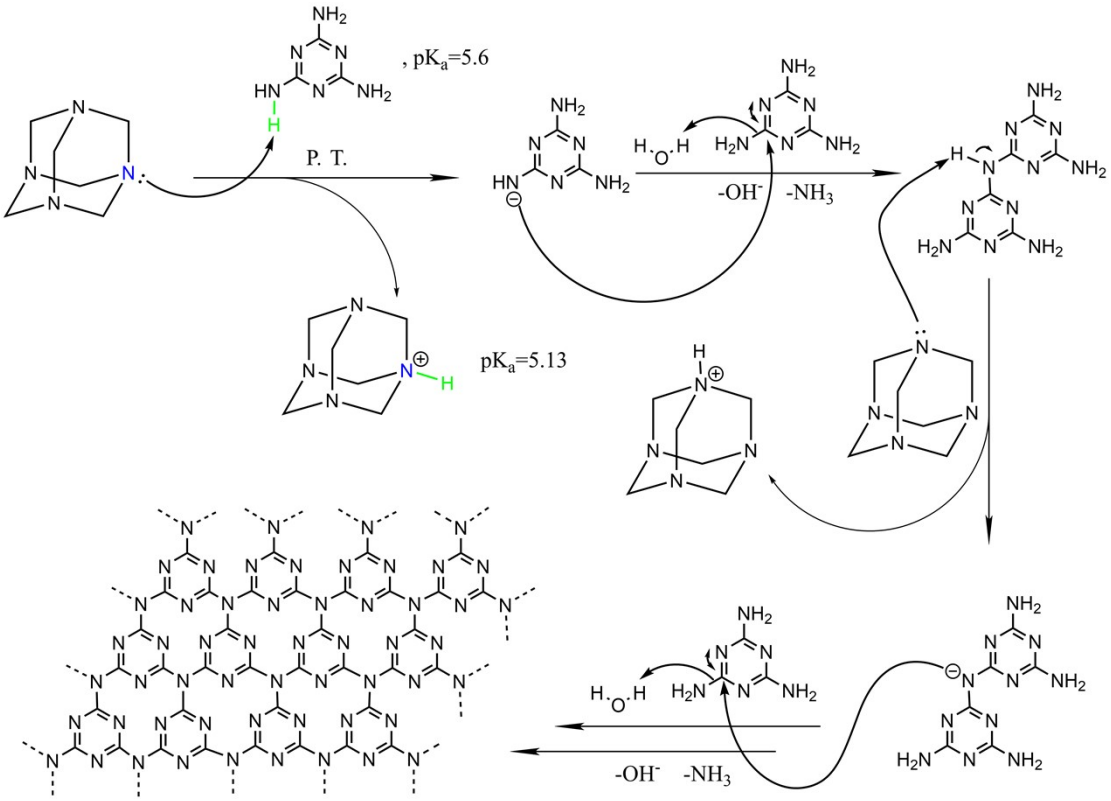

Fig. S1. Schematic illustration of synthesis process.

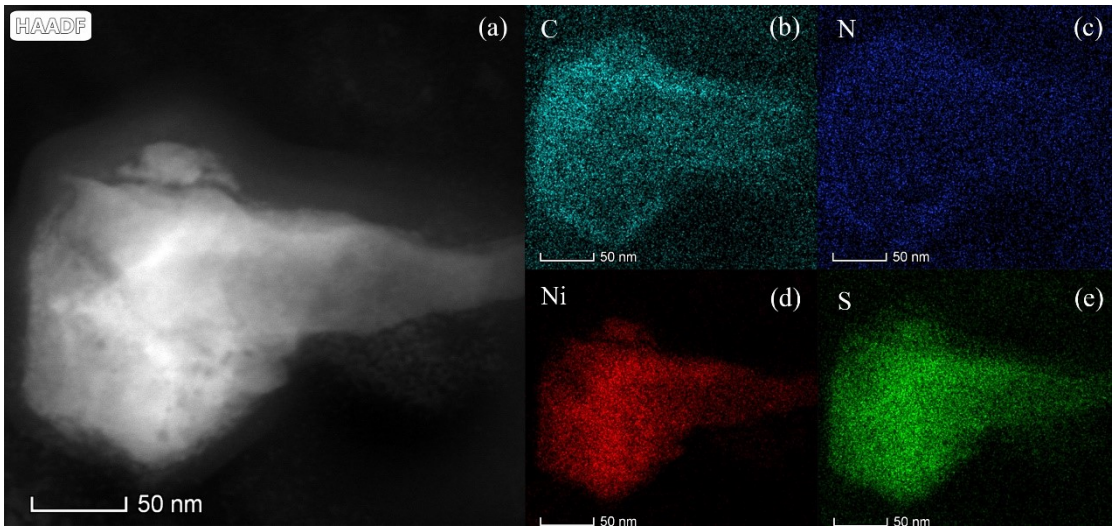

Fig. S2. (a) HAADF-TEM image of Ni_3S_2-NiS@g-C_3N_4, (b-e) element mapping of Ni_3S_2-NiS@g-C_3N_4.

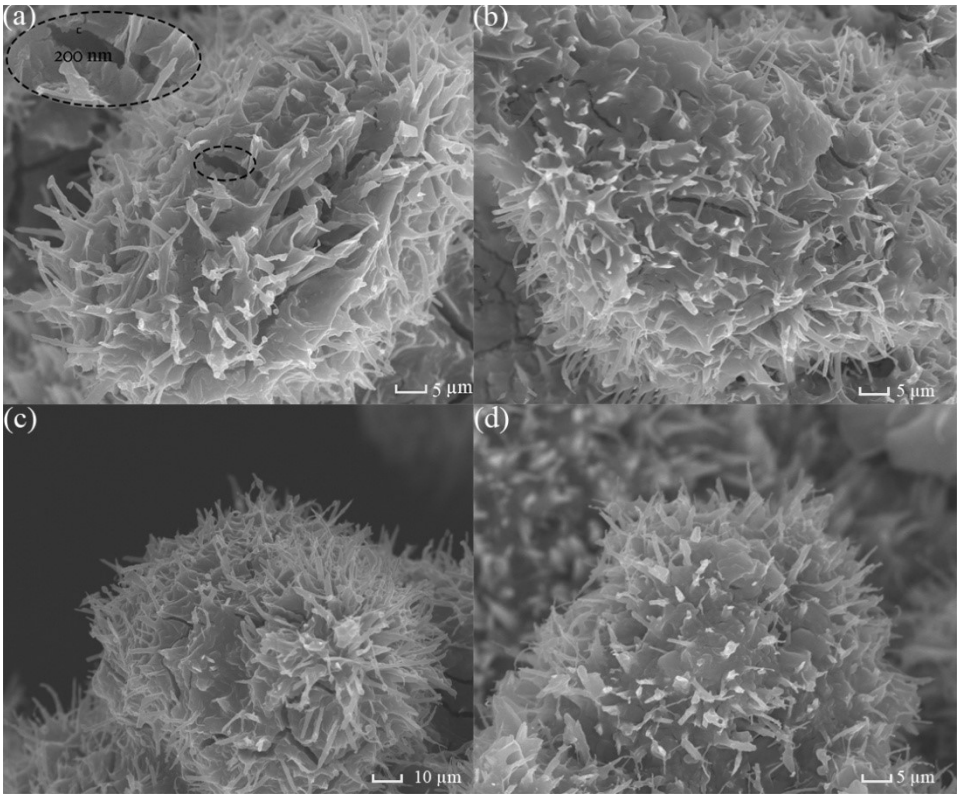

Fig. S3. SEM image of Ni_3S_2-NiS@g-C_3N_4

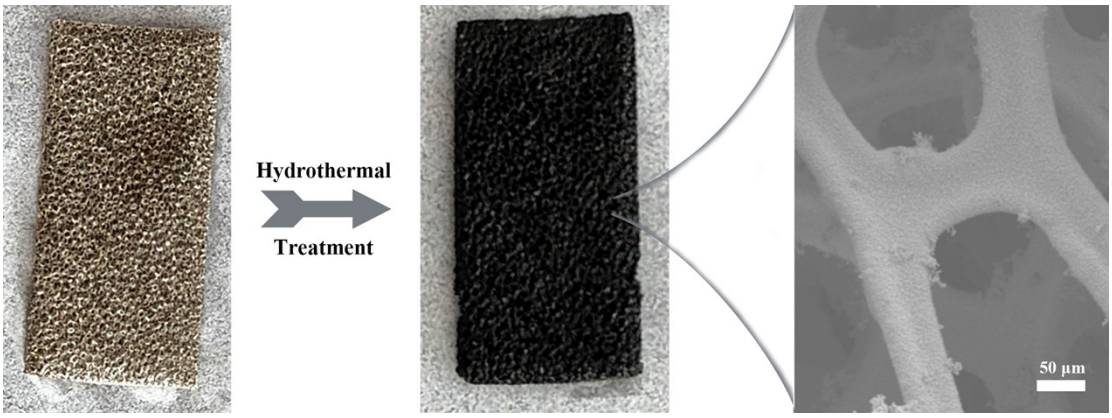

Fig. S4. Color changing and micro-SEM image of the NF after hydrothermal treatment.

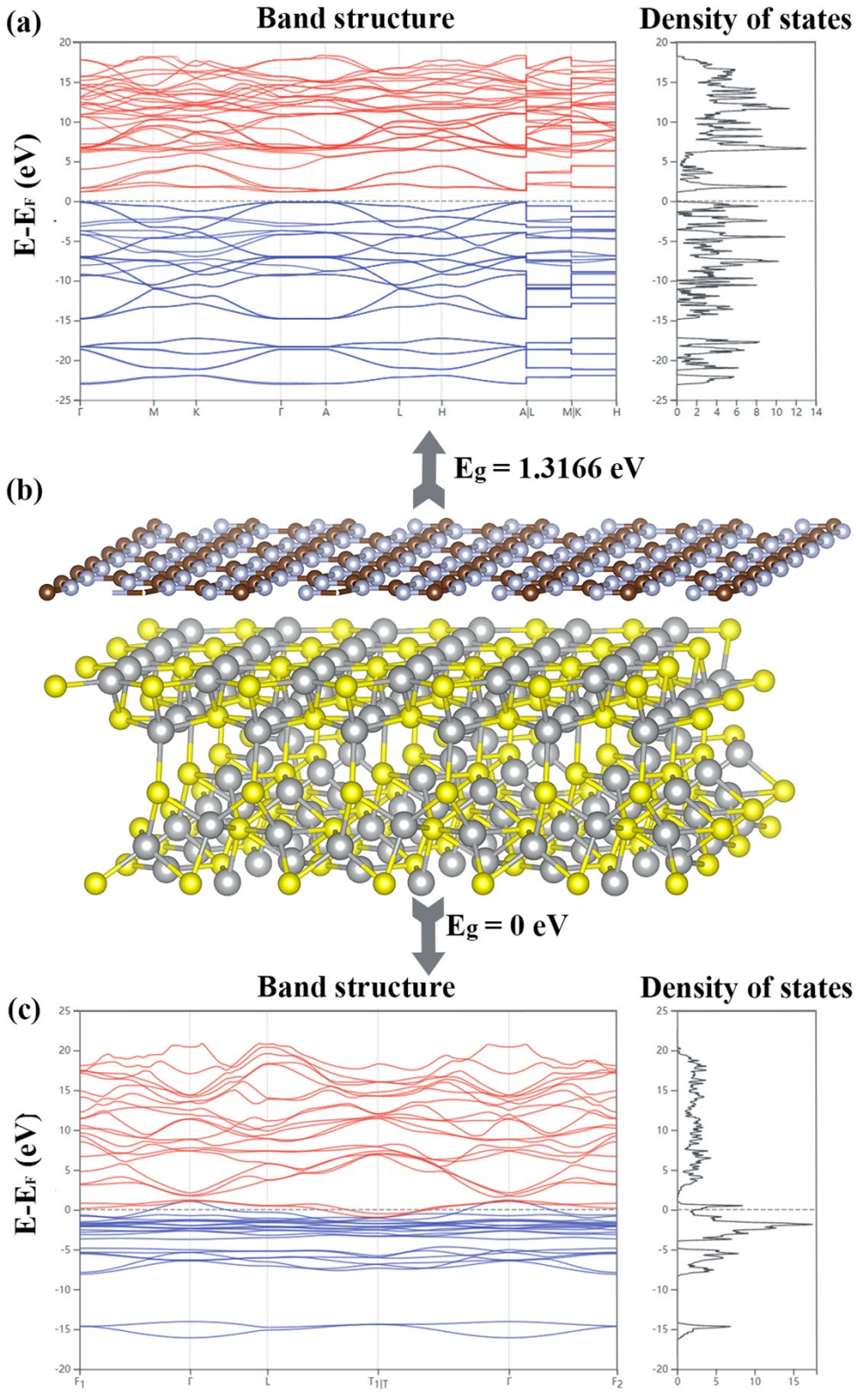

Fig. S5. (a) Band structure and density of states for the g-C_3N_4 part. (b) The model illustration of the g-C_3N_4 and NiS_x. (c) Band structure and density of states for the NiS_x part.

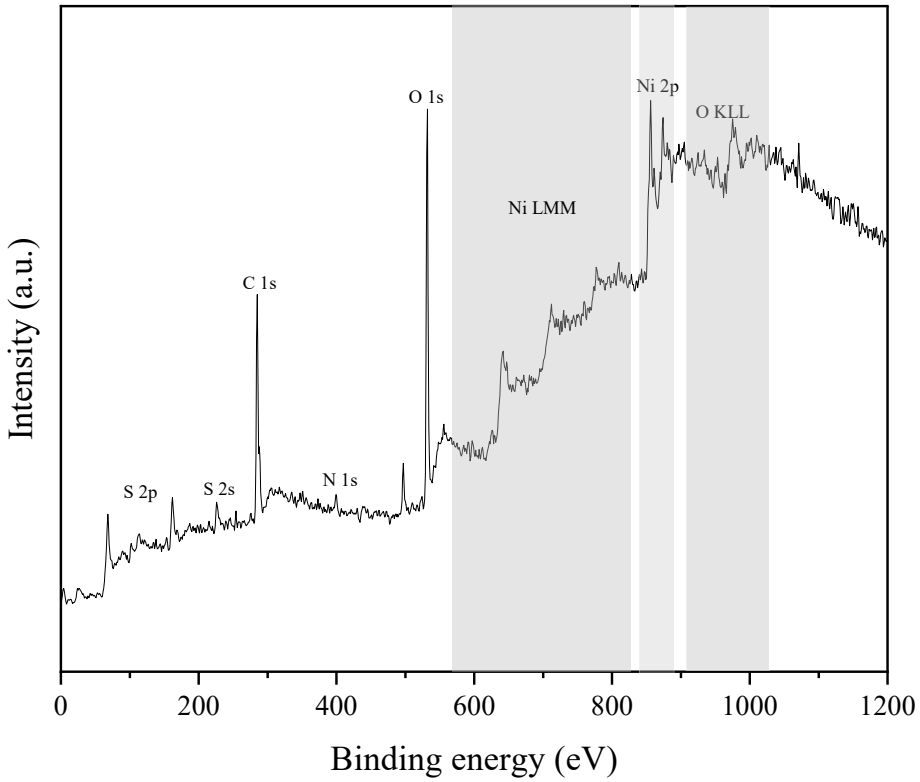

Fig. S6. Survey spectrum of Ni_3S_2-NiS@g-C_3N_4.

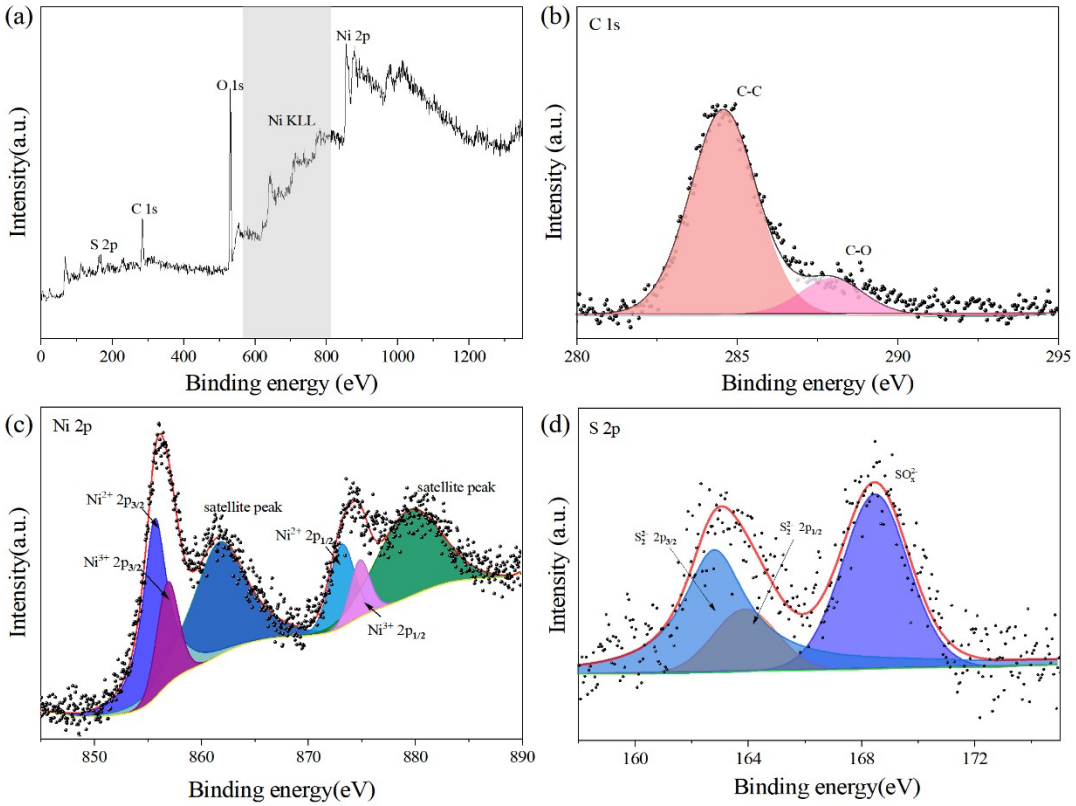

Fig. S7. (a) Survey spectrum, (b) C 1s, (c) Ni 2p, and (d) S 2p XPS patterns for Ni_3S_2 obtained without urotropine.

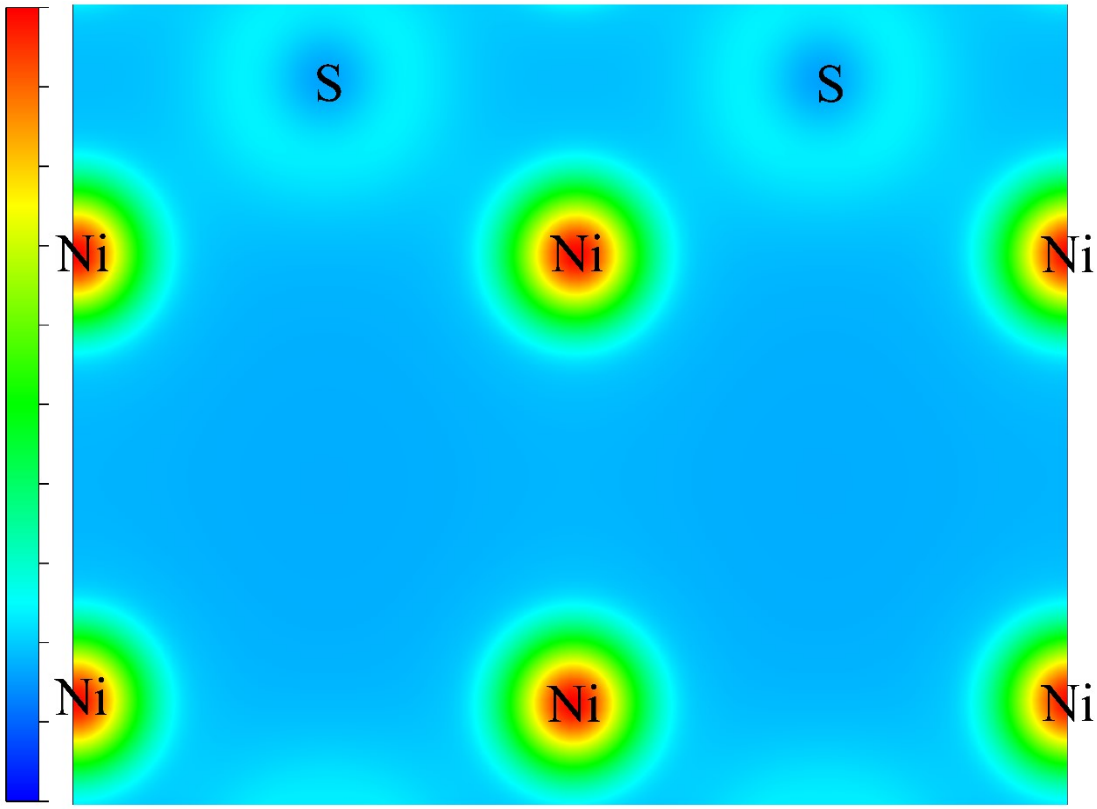

Fig. S8. Surface sliced charge different plot.

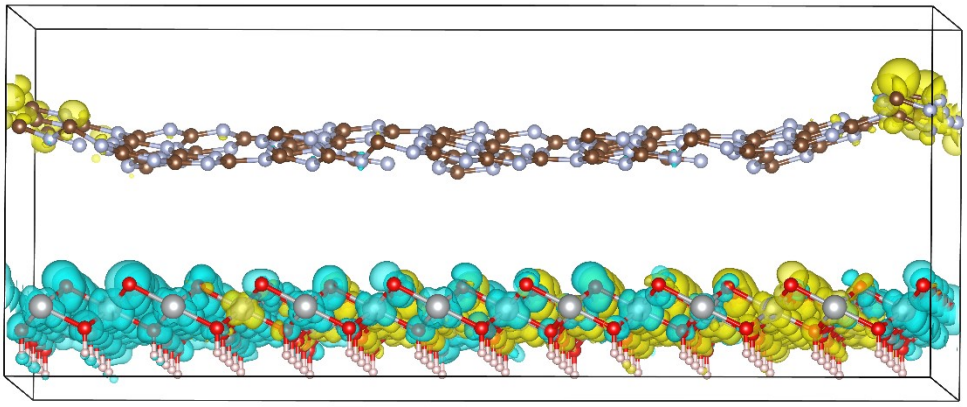

Fig. S9. Charge different plot for NiOOH@g-C_3N_4.

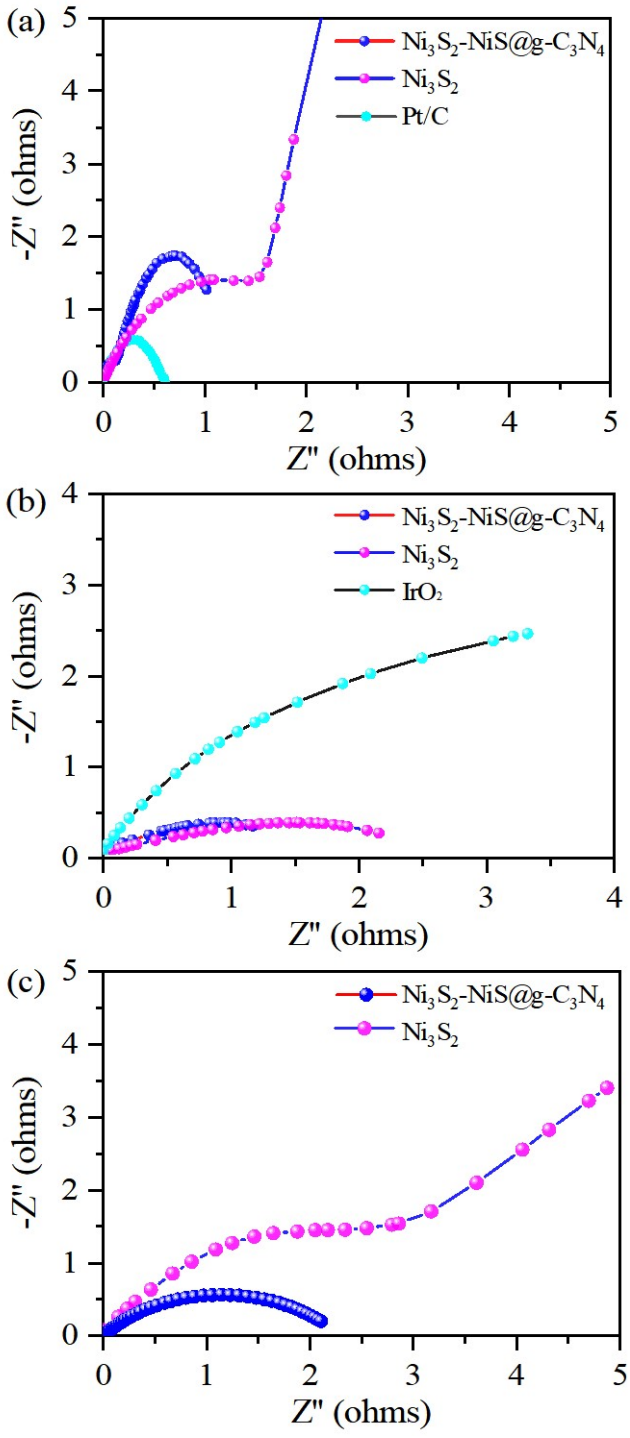

Fig. S10. EIS patterns for (a) HER, (b) OER, and (c) UOR.

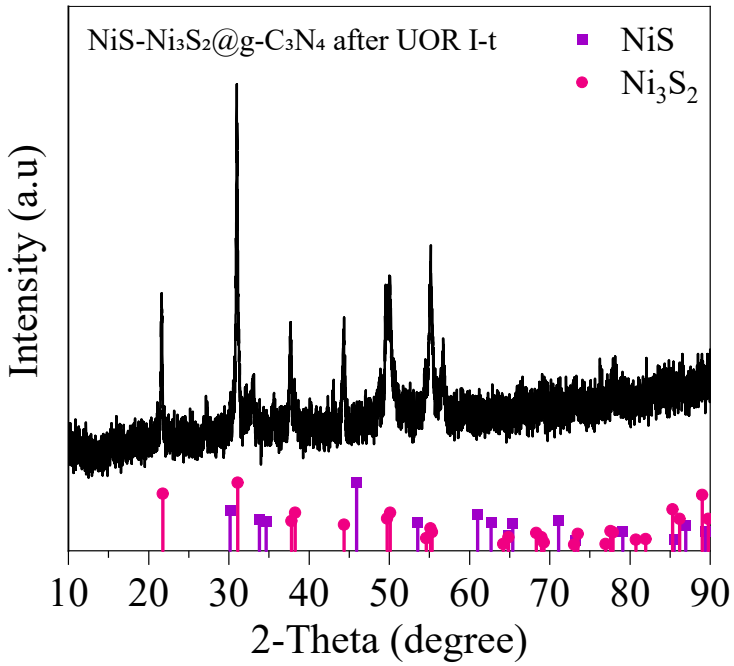

Fig. S11. XRD partners of Ni_3S_2 after UOR I-t test.

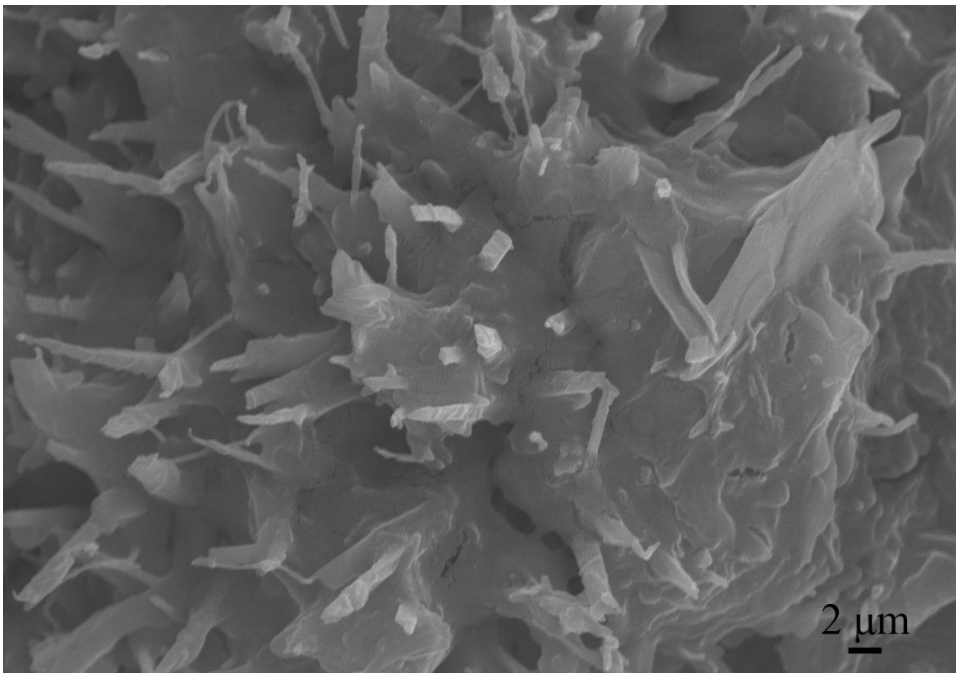

Fig. S12. SEM images of Ni_3S_2 after UOR I-t test.

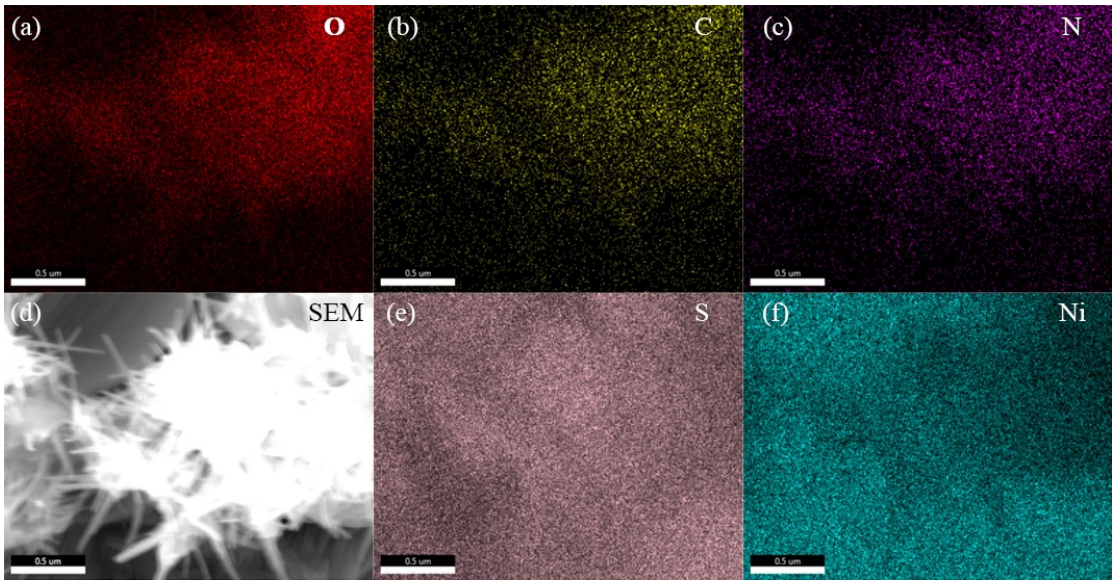

Fig. S13. (a-c, e, f) element mapping of Ni_3S_2-NiS@g-C_3N_4 after UOR test, (d) SEM image of Ni_3S_2-NiS@g-C_3N_4,

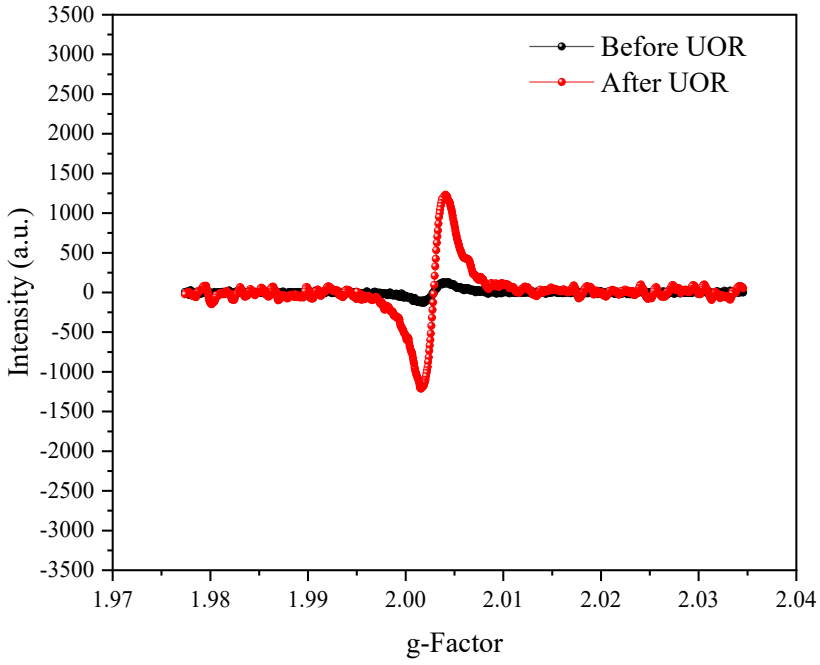

Fig. S14. EPR results for Ni_3S_2-NiS@g-C_3N_4 before and after UOR.

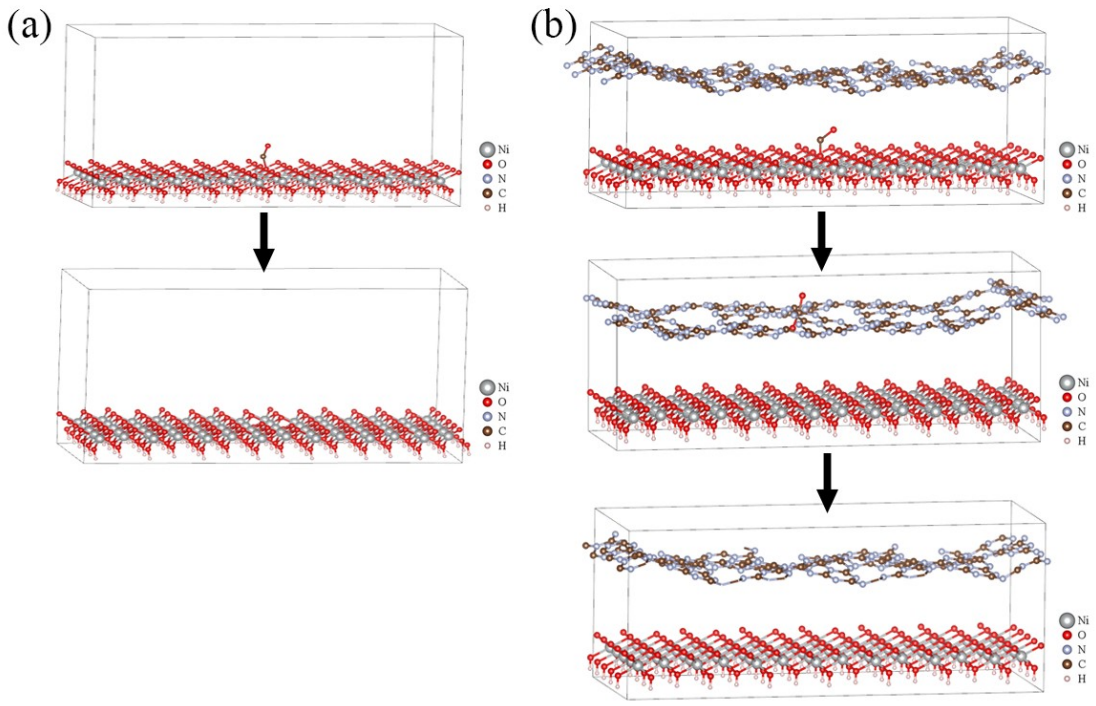

Fig. S15. The CO_2 transition process (a) without g-C_3N_4 membrane and (b) with g-C_3N_4 membrane.

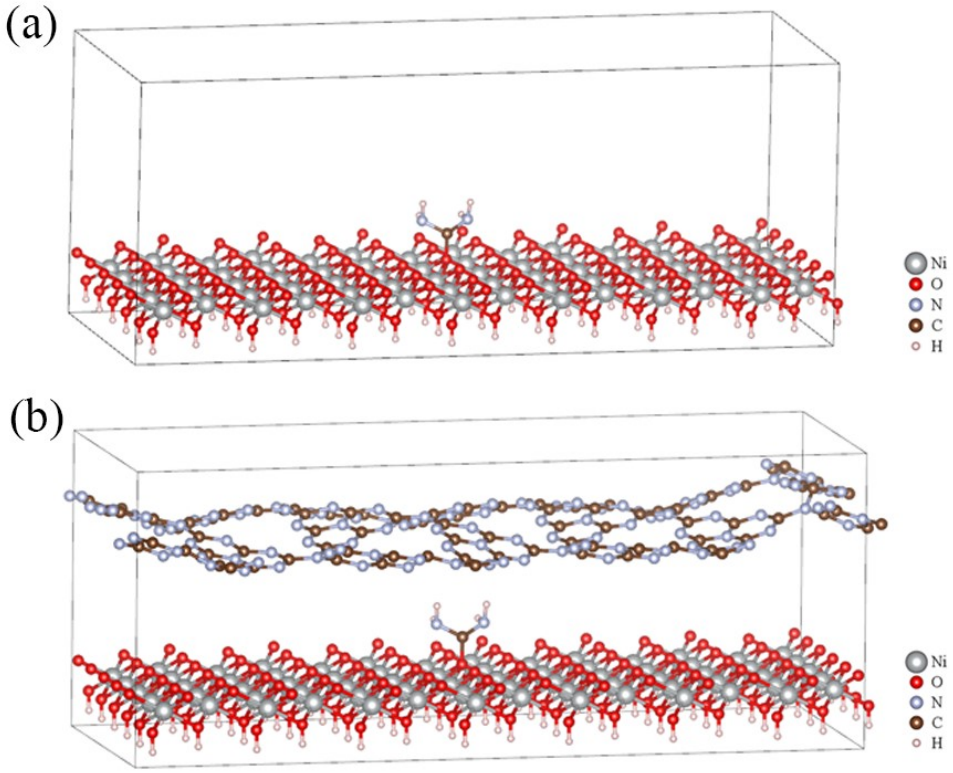

Fig. S16. Urea-adsorbed models (a) without urotropine and (b) with urotropine.

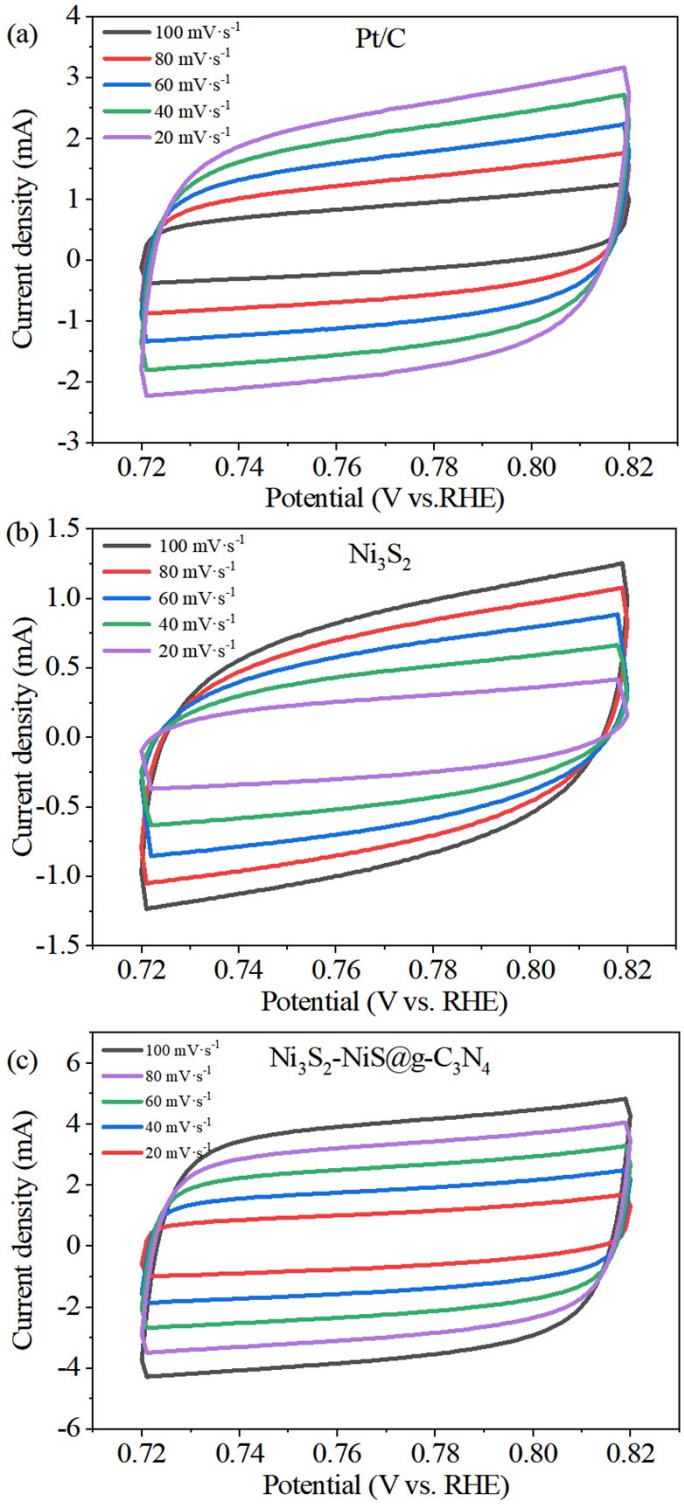

Fig. S17. C_{dl} curves of (a) Pt/C, (b) Ni_3S_2, and (c) Ni_3S_2-NiS@g-C_3N_4.

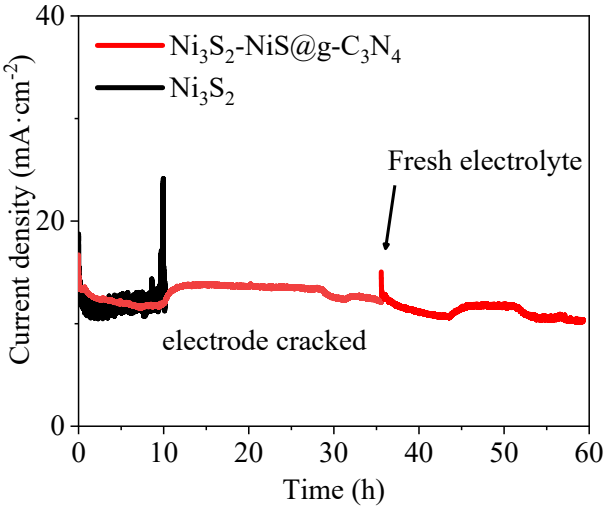

Fig. S18. I-t stability test of Ni_3S_2-NiS@g-C_3N_4 for OER.

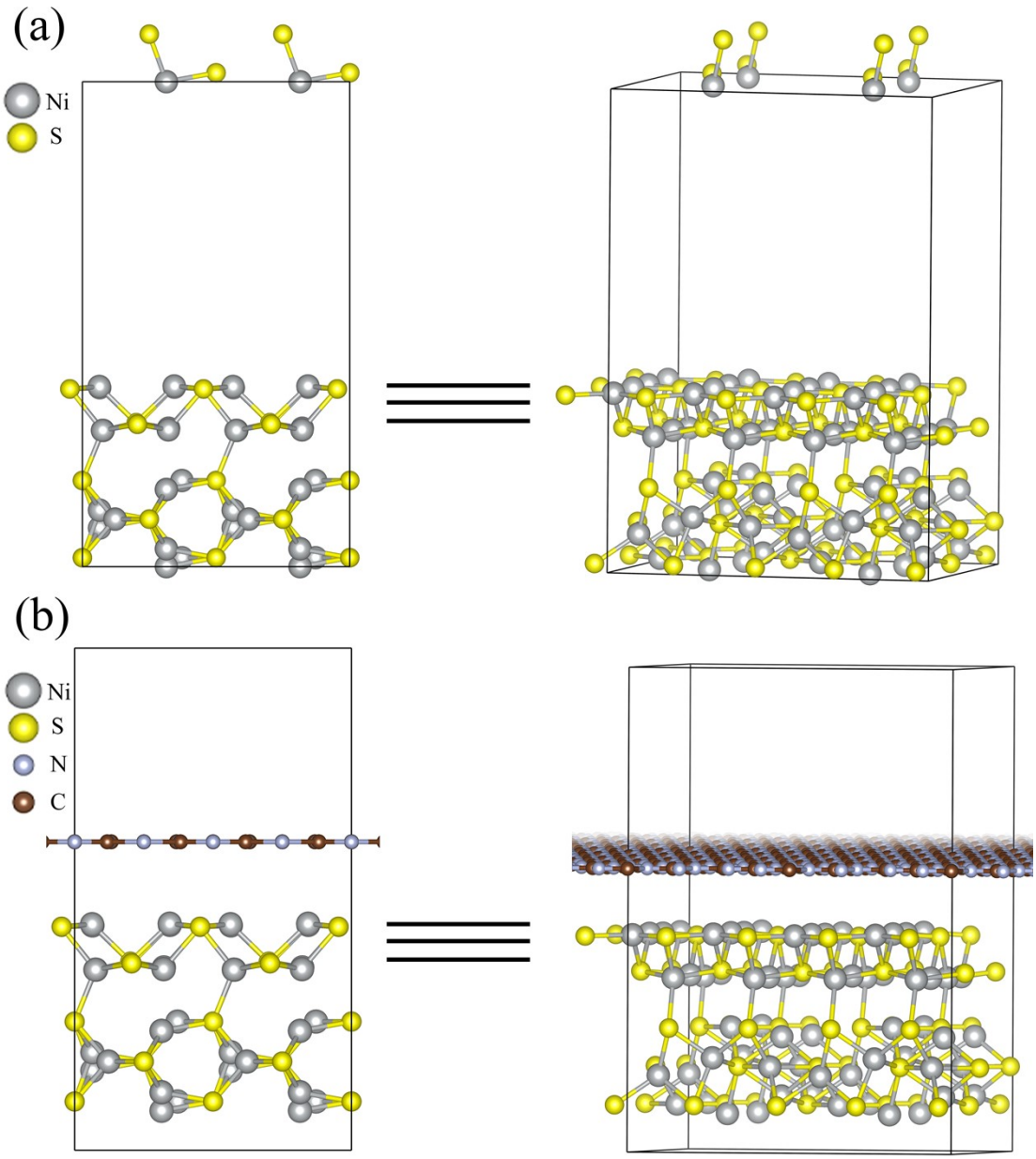

Fig. S19. HER model (a) without g-C_3N_4 membrane and (b) with g-C_3N_4 membrane.

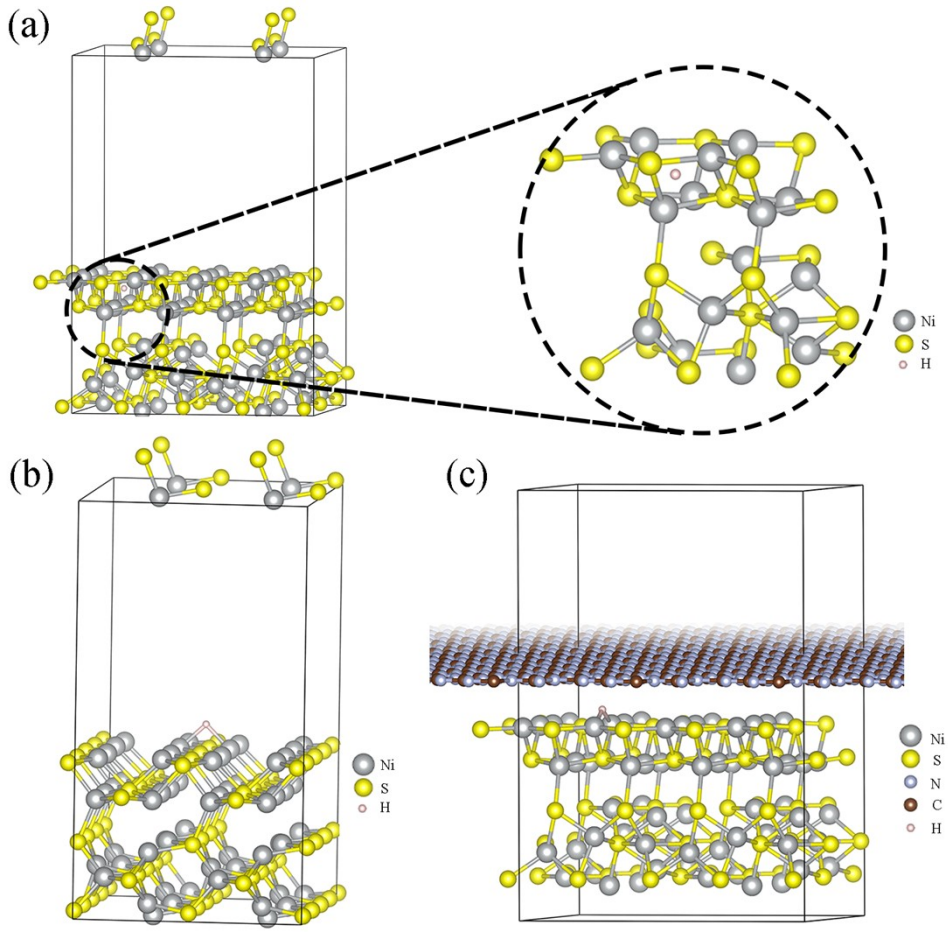

Fig. S20. (a) The model of HER site 1 without urotropine. (b) The model of HER site 2 without urotropine. (c) The model of HER site 1 with urotropine.

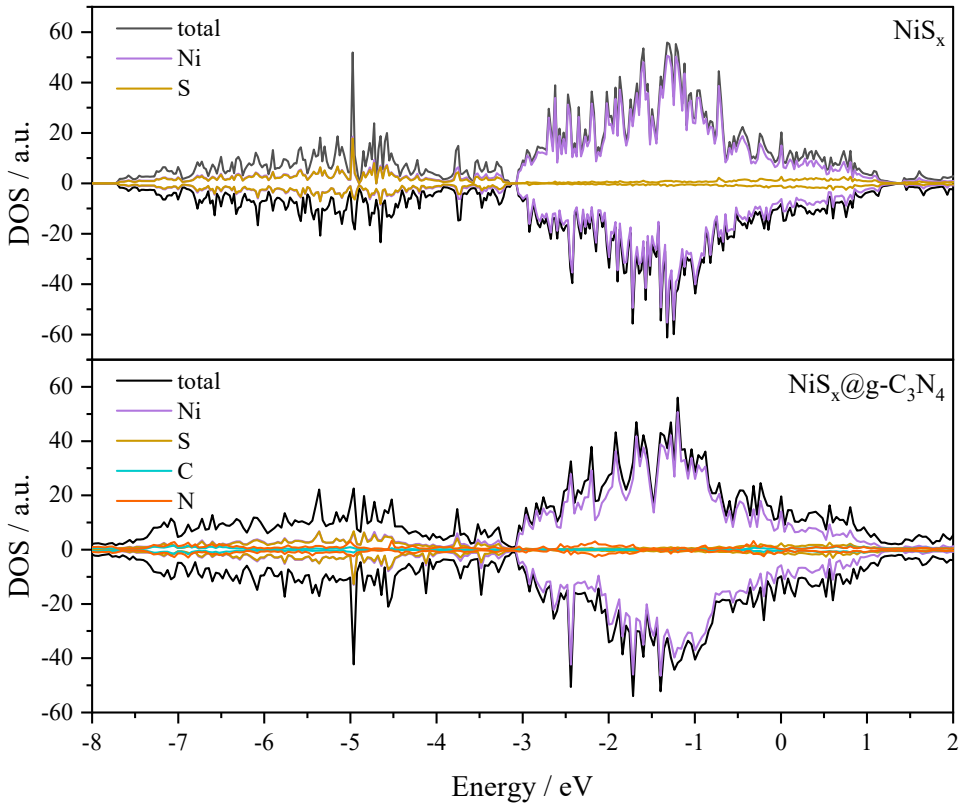

Fig. S21. DOS plots for HER model with and without g-C_3N_4.

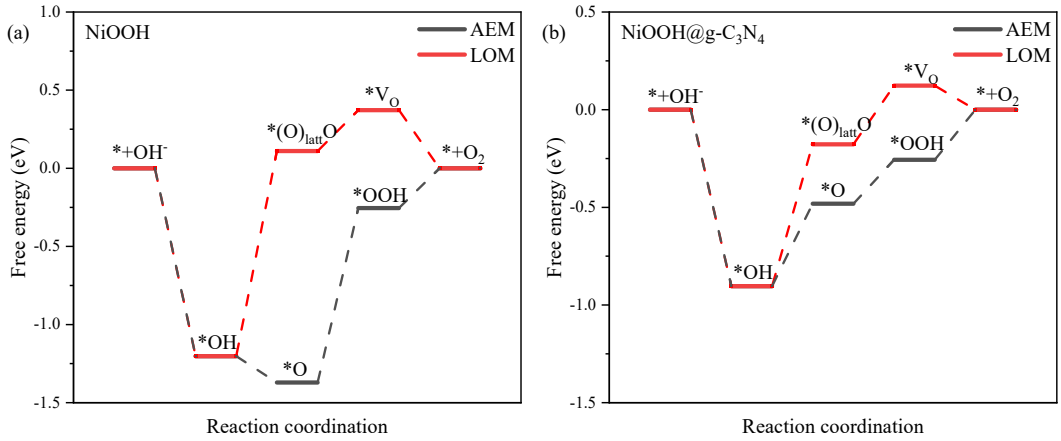

Fig. S22. The comparison between AEM and LOM pathway for (a) NiOOH and (b) NiOOH@g-C_3N_4.

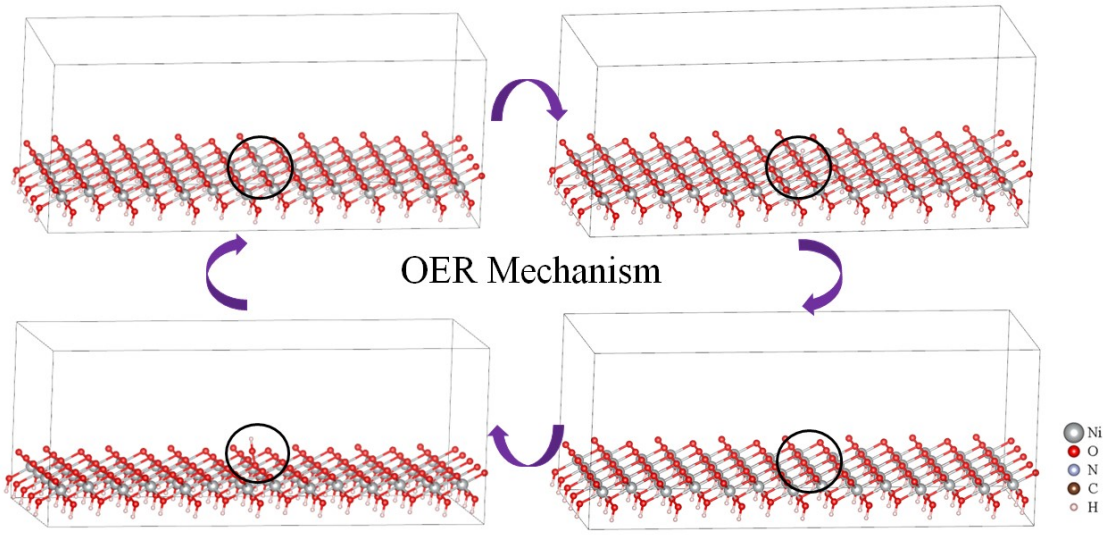

Fig. S23. The OER mechanism adopted in the paper.

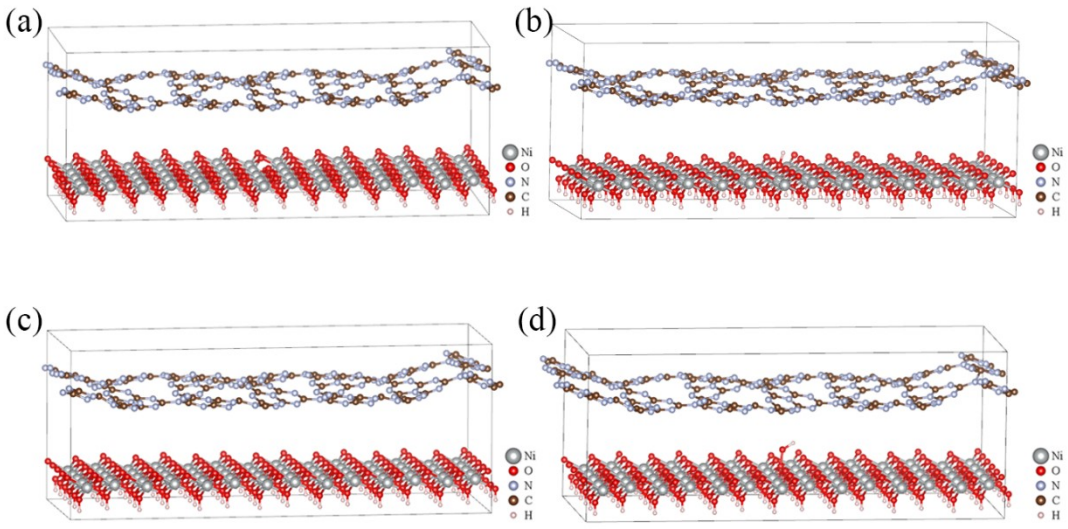

Fig. S24. (a) slab, (b) OH-adsorbed, (c) O-adsorbed, and (d) OOH-adsorbed models with urotropine for OER.

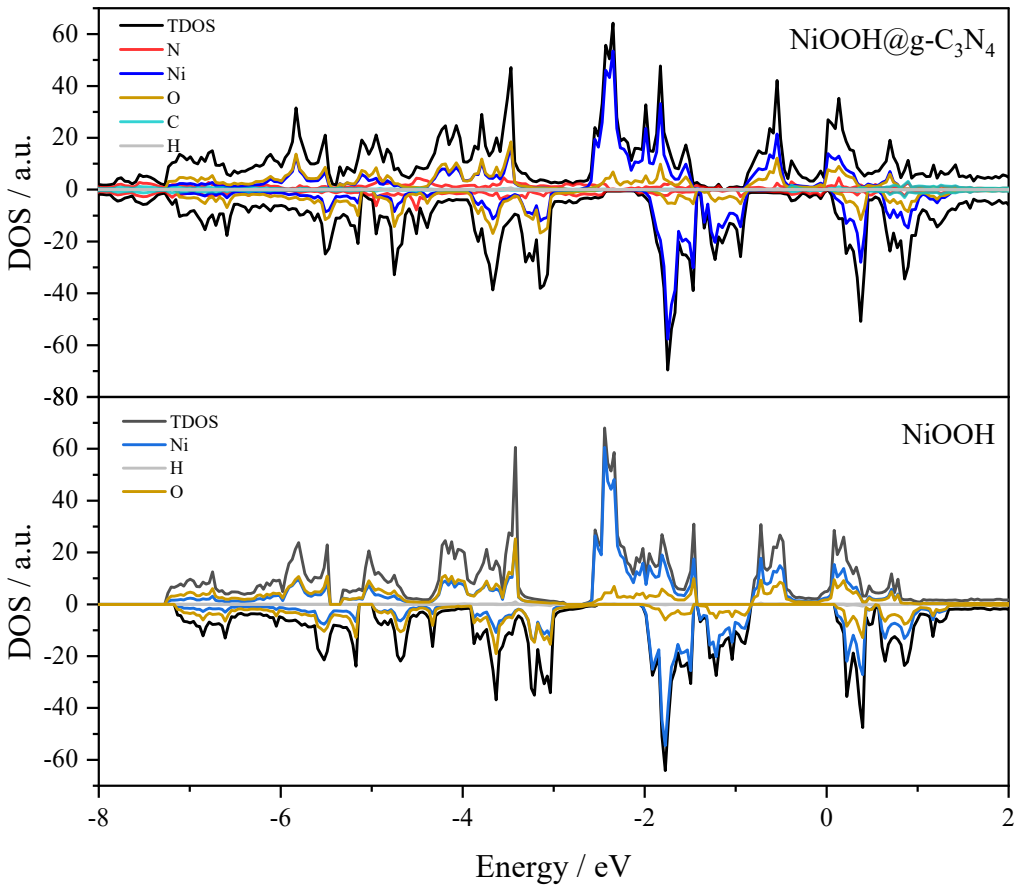

Fig. S25. DOS plots of NiOOH@g-C_3N_4 and NiOOH models.

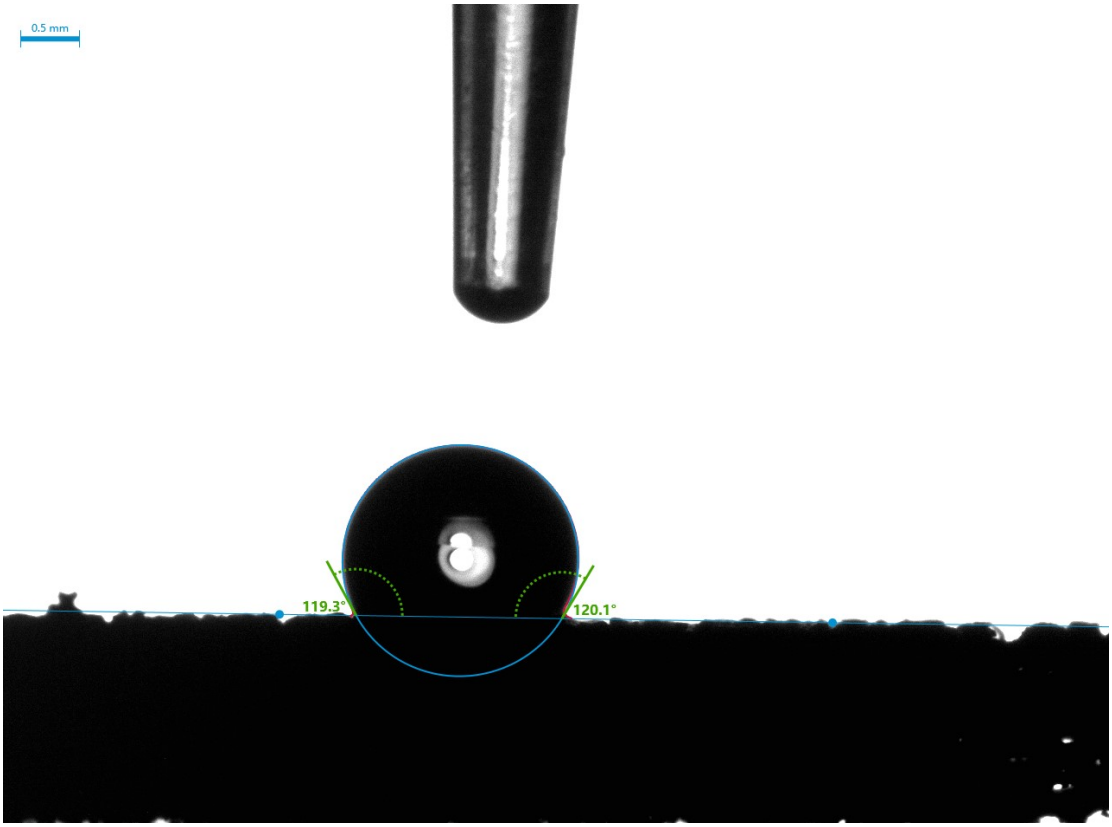

Fig. S26. Contact angle of the sample.

Table S1. Source of the raw materials used.

Materials	Specification	Source
nickel foam	1 cm × 1.5 cm	Kunshan Guangjiayuan New Materials Co., Ltd
HCl	1mol·L^{-1}	Aladdin Co., Ltd
thiourea	analytical pure, 99.9 %	Aladdin Co., Ltd
melamine	analytical pure, 99.9 %	Aladdin Co., Ltd
L-cysteine	analytical pure, 99.9 %	Aladdin Co., Ltd
$NiCl_2·6H_2O$	analytical pure, 99.9 %	Aladdin Co., Ltd

Table S2. The comparsion of Ni_3S_2-NiS@g-C_3N_4 with recent other HER catalysts.

Electrocatalysts	**E_{j10} for HER**	**E_{j100} for HER**	**Reference**
Co-Ni@Mo_4O_{11}	63 mV	220 mV	[1]
CoO/Mo_2C	107 mV	280 mV	[2]
MoS_2-Ni_3S_2 HNRs/NF	98 mV	198 mV	[3]
CoMoNiS-NF-xy	152 mV	350 mV	[4]
N-Ni_3S_2/NF	110 mV	330 mV	[5]
P-$NiCo_2S_4$@CNT/CNF	74 mV	230 mV	[6]
$Fe_{0.9}Ni_{2.1}S_2$@NF	72 mV	240 mV	[7]
Ni_3S_2/$FeNi_2S_4$	50 mV	260 mV	[8]
Ni_3S_2@$FeNi_2S_4$@NF	83 mV	270 mV	[9]
Ni_3S_2-NiS@g-C_3N_4	13 mV	204 mV	this work

Table S3. The comparsion of Ni_3S_2-NiS@g-C_3N_4 with recent other OER catalysts.

Electrocatalysts	**E_{j10} for OER**	**Reference**
CoO/Co_3O_4@NC	260 mV	[10]
MoS_2/Ni_3S_2 heterostructures	218 mV	[11]
MoS_2–Ni_3S_2 HNRs/NF	249 mV	[3]
CoMoNiS-NF-31	166 mV	[12]
Fe-Ni_3S_2/NF	310 mV	[13]
Ni_2P–Ni_3S_2 HNAs/NF	210 mV	[14]
Ni_3S_2-NiS@g-C_3N_4	90.9 mV	this work

Electrocatalysts	E_{onset}	E_{j100}	Stability	References
NiFe-MIL-53-NH_2	1.35	1.41	20 h @ 50 mA cm^{-1}	[15]
Ni nanowires	1.39	1.57	24 h @ 5 mA cm^{-1}	[16]
Ni nanowire arrays	1.33	1.43	3 h @ 20 mA cm^{-1}	[17]
NC600/Ti	1.328	1.38	5 h @ 120 mA cm^{-1}	[18]
NiFe NSs	1.31	1.37	24 h @ 10 mA cm^{-1}	[19]
Ni-Sn	1.313	1.56	12 h @ 10 mA cm^{-1}	[20]
Ni-W_5N_4-NF	1.312	1.38	130 h @ 10 mA cm^{-1}	[21]
Ni-Bi	1.291	---	3 h @ 10 mA cm^{-1}	[22]
C-NiCo CHs	1.377	1.7	20 h @ 70 mA cm^{-1}	[23]
Ni_3S_2-NiS@g-C_3N_4	1.24	1.34	48 h @ 10 mA cm^{-1}	this work

Table S4. The comparsion of Ni_3S_2-NiS@g-C_3N_4 with recent other UOR catalysts.

References

[1] Islam, M. Jena, S. Sidra, S. Thanh Tran, D. Hwan Kim, D. Hoon Kim, N. Hee Lee, J. Chemical Engineering Journal 2024, 487, 150664.

[2] Chen, H.-Y. Yang, L. Wang, R.-X. Zhang, W.-J. Liu, R.; Yun, Y.-Z. Wang, N.; Ramakrishna, S.; Jiao, L.; Long, Y.-Z., Small 2023, 19 (49), 2304086.

[3] Yang, Y. Zhang, K. Lin, H. Li, X. Chan, H. C. Yang, L. Gao, Q. ACS Catalysis 2017, 7 (4), 2357-2366.

[4] Yang, Y. Yao, H. Yu, Z. Islam, S. M. He, H. Yuan, M. Yue, Y. Xu, K. Hao, W. Sun, G. Li, H. Ma, S. Zapol, P. Kanatzidis, M. G. Journal of the American Chemical Society 2019, 141 (26), 10417-10430.

[5] Li, B. Li, Z. Pang, Q. Electrochimica Acta 2021, 399, 139408.

[6] Gu, H. Fan, W. Liu, T. Nanoscale Horizons 2017, 2 (5), 277-283.

[7] Fei, B. Chen, Z. Liu, J. Xu, H. Yan, X. Qing, H. Chen, M. Wu, R. Advanced Energy Materials 2020, 10 (41), 2001963.

[8] Wu, Y. Li, Y. Yuan, M. Hao, H. San, X. Lv, Z. Xu, L. Wei, B. Chemical Engineering Journal 2022, 427, 131944.

[9] Yang, Y. Meng, H. Kong, C. Yan, S. Ma, W. Zhu, H. Ma, F. Wang, C. Hu, Z. Journal of Colloid and Interface Science 2021, 599, 300-312.

[10] Zhang, K. Li, N. Weng, Y. Kang, Y. Lee, J. Y. Zhang, H. Ding, Y. Han, X. Pang, H. Advanced Functional Materials 2025, 2507212.

[11] Zhang, J. Wang, T. Pohl, D. Rellinghaus, B. Dong, R. Liu, S. Zhuang, X. Feng, X. Angewandte Chemie International Edition 2016, 55 (23), 6702-6707.

[12] Yang, Y. Yao, H. Yu, Z. Islam, S. M. He, H. Yuan, M. Yue, Y. Xu, K. Hao, W. Sun, G. Li, H. Ma, S. Zapol, P. Kanatzidis, M. G., Journal of the American Chemical Society 2019, 141 (26), 10417-10430.

[13] Xie, N. Ma, D.-D. Wu, X.-T. Zhu, Q.-L. Nanoscale 2021, 13 (3), 1807-1812.

[14] Zeng, L. Sun, K. Wang, X. Liu, Y. Pan, Y. Liu, Z. Cao, D. Song, Y. Liu, S. Liu, C. Nano Energy 2018, 51, 26-36.
[15] Gao, Z. Wang, Y. Xu, L. Tao, Q. Wang, X. Zhou, Z. Luo, Y. Yu, J. Huang, Y. Chemical Engineering Journal 2022, 433, 133515.
[16] Yan, W. Wang, D. Diaz, L. A. Botte, G. G. Electrochimica Acta 2014, 134, 266-271.
[17] Guo, F. Ye, K. Cheng, K. Wang, G. Cao, D. Journal of Power Sources 2015, 278, 562-568.
[18] Gao, X. Wang, Y. Li, W. Li, F. Arandiyan, H. Sun, H. Chen, Y. Electrochimica Acta 2018, 283, 1277-1283.
[19] Diao, Y. Liu, Y. Hu, G. Zhao, Y. Qian, Y. Wang, H. Shi, Y. Li, Z. Biosensors and Bioelectronics 2022, 211, 114380.
[20] Ji, Z. Liu, J. Deng, Y. Zhang, S. Zhang, Z. Du, P. Zhao, Y. Lu, X. Journal of Materials Chemistry A 2020, 8 (29), 14680-14689.
[21] Zhou, Y. Chu, B. Sun, Z. Dong, L. Wang, F. Li, B. Fan, M. Chen, Z. Applied Catalysis B: Environmental 2023, 323, 122168.
[22] Munde, A. V. Mulik, B. B. Dighole, R. P. Sathe, B. R. ACS Applied Energy Materials 2021, 4 (11), 13172-13182.
[23] Khalafallah, D. Ouyang, C. Zhi, M. Hong, Z. ChemCatChem 2020, 12 (8), 2283-2294.